IEEE Access
Multidisciplinary | Rapid Review | Open Access Journal

Received October 15, 2019, accepted November 23, 2019, date of publication November 27, 2019,
date of current version December 12, 2019.

Digital Object Identifier 10.1109/ACCESS.2019.2956289

Entropy Method for Structural Health Monitoring Based on Statistical Cause and Effect Analysis of Acoustic Emission and Vibration Signals

KAI TAO[1,2], WEI ZHENG[1], (Member, IEEE), AND DANCHI JIANG[2], (Member, IEEE)

[1]Key Laboratory for Optoelectronic Technology and System of the Education Ministry of China, College of Optoelectronic Engineering, Chongqing University, Chongqing 400044, China

[2]School of Engineering, University of Tasmania, Hobart, TAS 7001, Australia

Corresponding author: Wei Zheng (zw3475@163.com)

This work was supported in part by the National Natural Science Foundation of China under Grant 61573073, and in part by the China Scholarship Council under Grant 201806050136.

ABSTRACT Acoustic emission (AE) and vibration signal are significant criteria of damage identification in structural health monitoring (SHM) engineering. Multi-disciplinary knowledge and synergistic parameter effects are technical challenges for damage assessment modelling. This study proposes a structural damage cause-and-effect analysis method based on parameter information entropy. Monitoring data is used to form a time-domain feature wave (TFW). The structural strength degradation factor (DF) would be used to define structural damage information entropy (SDIE) vector. The structural damage cause and effect model is developed in a probability sense. A fatigue index is adopted for damage assessment, and a causal strength index is proposed to locate the most likely damage cause. A sandstone-truss structure experiment was conducted to show that the proposed method is effective for damage evaluation and the experimental results provide strong support. This is a statistical damage identification method based on causal logic uncertainty, meaning a complicated mechanics calculation can be avoided.

INDEX TERMS Structural health monitoring, acoustic emission, cause-and-effect analysis, parameter information entropy.

I. INTRODUCTION

Structural health monitoring (SHM) is significant to ensure engineering system safety. Damage evaluation system detects the physical parameter changes using sensors. The structural data changes are monitored through mathematical models and intelligent algorithms. Subsequently, the safety status is evaluated combining structural features and environmental impacts [1]. In addition to the monitoring of abnormal parameter changes, the damage level assessment, damage cause identification and locating, etc., are also significant issues in SHM. Furthermore, issues such as sensor aging, reliability reduction, and data loss would occur due to unexpected harsh environment. Thus, an ideal monitoring system should be adaptive to environment changes. The parameter learning and data intelligence mining are also necessary functions [2], [3].

The associate editor coordinating the review of this manuscript and approving it for publication was Chao Tan.

Acoustic emission (AE) is a physical consequence that the structure releases elastic waves to reach a steady state when subjected to stress [4]. The AE signal contains a rich variety of structural damage information [5] and has been widely used in fault diagnosis engineering [6]–[8]. Parametric analysis (PA) has been frequently used in SHM in areas such as bridge construction, mechanical wear, and tool flaw detection [9]–[12]. Conventional damage assessment methods are usually based on signal frequency domain analysis (such as Wavelet transform (WT), fast Fourier transformation (FFT)) and time domain analysis (such as autoregressive model with exogenous input (ARX), eigensystem realization algorithm (ERA)), etc [13]–[16]. As monitoring data expands, the required storage capacity and computing power increases. Pattern recognition based on the logical association between sensor data and damage has become a viable solution in recent years. Various network models have been developed for different damage issues. For example, in [17] the logical associations between AE energy, cracking

damage and environmental noise were investigated. Based on that, damage in a welded steel pipe was successfully detected through the Bayesian theory. In [18] a non-linear localization framework was proposed to localize acoustic emission sources. In [19] an adaptive neuro-fuzzy inference system was integrated to quantify the damage index accurately. In [20] a machine learning framework integrating multiple intelligent algorithms for aircraft damage identification was developed, where simulation experiments were also included to show the advantages of this model in strategy reliability and harvested energy. Vibration is a basic physical reaction of structure destruction. Damage information can be reflected well by features extracted from vibration signals. Vibration-based methods, such as modal analysis, frequency-time domain analysis, impedance analysis, etc., are significant tools in SHM engineering. Much research has been done using vibration analysis methods. In [21] a vibration-based damage detection method was proposed through vibration model identification theory. An application example showed that this method is suitable for complicated structures with no parameters available. In [22] a modal parameter tracking system was deployed on an arch bridge for long-time damage monitoring. The feasibility of the monitoring strategy was demonstrated combined with intelligent algorithms. In [23] two types of features were extracted from the damage signal. The numerical example showed that output-only vibration measurement problems can be solved under changing environmental conditions.

Actual engineering damage can be caused by a combination of diverse environmental factors (EFs). Damage occurs randomly as the accumulative consequence of various EFs over time and space. The monitored physical parameters and structural damage are usually coupled and one is related to the other. However, there is not sufficient existing literature available that discusses the such relationship between damage and EF in a multi-disciplinary way systematically. The profound relationships among damage level, monitored parameters and EF are still worth investigating and the technical reasons are as follows:

a). Synergistic effect exists between the damage events and EFs. A damage event may be caused by multiple EFs, and an EF can cause multiple damage events. For example, structure brittleness can be affected by many EFs, including temperature, humidity, and stress. On the other hand, in addition to stiffness decreases, potential of hydrogen (PH) can also cause damage such as cracking displacement and local expansion. There are multidimensional disparities in monitored parameters and damage types. The specific relationship between each parameter and damage depends on multidisciplinary areas such as structural mechanics, geotechnical mechanics, and materials science. Thus, the resultant model can be extremely complicated combining multiple facades of such a system.

b). Signal parameters are diverse, and the structural characteristics reflected by each parameter can be quite different. The appropriate parameter types may vary with the application scenario and environmental conditions. Conventional signal parameter selecting methods tend to be subjective and lack universal standards.

c). The occurrence of damage is also a random event governed by unidentified probabilistic models. An EF may not cause direct structural damage, but it can increase the probability of safety-affecting accidents. Structural damage is a macroscopic consequence of cumulative EFs in many aspects. The determination of the relationship between EF and damage is critically dependent on the rationality of assessment results. The diversity and possible inconsistency among multiple factors, including monitoring mathematical model complexity, a multidisciplinary knowledge framework, local cluster computing power, and system portability can be technical challenges for the investigation of a SHM system.

Damage is caused by cumulative EFs randomly, and the structural health degradation process and the associated causes can be reflected in the historical damage data. For the sake of reciprocal analysis between damage events and EF with multi-parameter integrated influence, a structural damage cause-and-effect analysis model based on parameter information entropy is proposed in this study. This model quantifies the damage occurrence from the perspective of probability uncertainty. A time-domain feature wave (TFW) is created according to the signal parameters, and then the structural damage information entropy (SDIE) is defined to represent the structural damage level based on a strength degradation factor (DF) matrix. Furthermore, fatigue index and causal strength index are proposed to characterise the possibility of damage caused by an EF. Based on that, both damage level assessment and identification of the most likely cause and location can be obtained. This method combines the statistical causal analysis and the basic engineering parameters. Multi-dimensional monitoring data is processed collaboratively. The damage assessment and location can be conducted only using the basic physical parameters. Compared with traditional damage signal processing methods (such as Moment tensor, Artificial neural networks), the uncertainty information of multiple damage factors can be considered synergistically. Complex calculations such as constitutive equations, vibration characteristics analysis, multi-physics coupling effect, etc., are not required.

II. METHODOLOGY

The model for basement damage assessment and the most likely cause identification and location of sandstone-truss structure is considered to illustrate our proposed method. AE signal is collected, and the feature parameters are calculated to obtain the judgements used for damage assessment. Since only the arrival time of vibration signal is captured for damage locating, the parameters extraction is not required. In this section, original signals are stacked into a TFW which contains all parameter information over time. The uncertainty of damage is estimated through calculating the parameter interval, the DF matrix, and the SDIE vector.

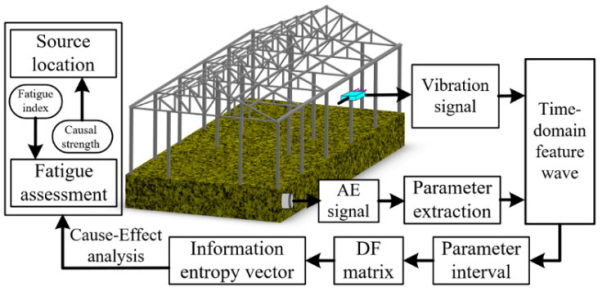

FIGURE 1. The procedure of the model.

Finally, cause-and-effect analysis is carried out. The severity of damage degree is assessed based on a fatigue index, and the most likely damage cause is represented using a causal strength index. The procedure is shown in Fig 1.

A. TIME-DOMAIN FEATURE WAVE

Let a set of SHM system acoustic signals collected at a given appropriate sampling frequency be denoted as $\boldsymbol{A}(A_1, A_2, \ldots A_{num})$, where *num* is the number of monitoring nodes. For a node z, the time domain monitoring signal can be represented as $\boldsymbol{A_z}(a_1, a_2, \ldots a_n)$, where n is the number of samples. Signals can be further analyzed to obtain time and frequency domain feature parameters, such as energy, mean, peak frequency and so on. Assume that the parameter matrix obtained from the monitoring signal is $\boldsymbol{B}(b_1, b_2, \ldots b_m)$, where m is the number of feature parameters. It can be represented in the time domain as follows:

$$B = \begin{bmatrix} b_{11} & b_{12} & \ldots & b_{1l} \\ b_{21} & \ldots & \ldots & b_{2l} \\ \ldots & \ldots & \ldots & \ldots \\ b_{m1} & \ldots & \ldots & b_{ml} \end{bmatrix}, \quad (1)$$

where l is the number of valid signal segments. For a feature parameter i, the parameter vector can be expressed as $\boldsymbol{B_i}(b_{i1}, b_{i2}, \ldots b_{im})$.

Conventional PA methods discuss the changes of a single parameter under external excitation in a time sequence. Even though these methods can well reflect the response of a single parameter to an EF, it is desirable to improve the following aspects for overall damage assessment:

a.) The dominating feature parameter set may change significantly with only some of the environmental stimuli. However, appropriate parameter selection to capture those stimuli largely relies on expert's skills and experience.

b.) The damage level assessment is obtained based on many specific parameters. Even though these parameters can easily be isolated, there lacks reasonable insight to reveal their relationship.

To collectively analyse multi-parameter effects in damage assessment over time, the original signal is converted to a TFW containing the parameter information during the entire time interval of interest. Each row of the parameter matrix $\boldsymbol{B}$ represents one parameter sample sequence. Each row of $\boldsymbol{B^T}$ is defined as a TFW unit and a TFW vector $\boldsymbol{B_{TF}}$ is defined as the row vector $(b_{11}, b_{21}, \ldots b_{m1}; b_{12}, b_{22}, \ldots b_{m2}; \ldots; b_{1h}, b_{2h}, \ldots b_{mh}; \ldots; b_{1l}, b_{2l}, \ldots b_{ml})$, where $h \in [1, l]$. The TFW vectors are homogenous in the time domain. Though TFW is a combination of various parameters, its parameter components are consistent with the conventional parameter matrix in the time domain. Thus, the conventional time domain analysis algorithms are still feasible.

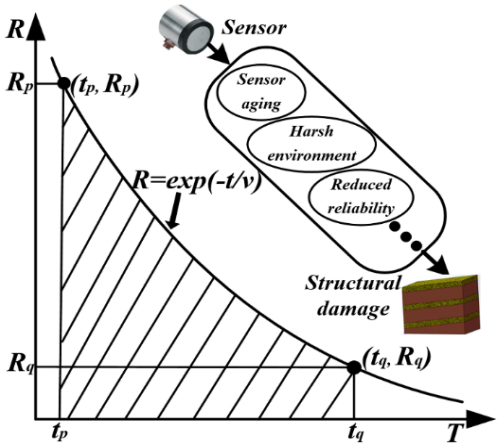

FIGURE 2. Structural degradation flow curve.

B. STRUCTURAL STRENGTH DEGRADATION FACTOR (DF) MATRIX

Consider SHM systems situated in structurally critical areas, usually under high temperatures, and subject to pressure and stress constraints. Harsh monitoring environments cause numerous problems for damage detection systems which use the sensor output as the underlying data source. Issues such as sensor aging, reliability reduction, and information loss are challenges for accurate disaster prediction. In this paper, a damage evaluation method based on cause-and-effect analysis was proposed. The detailed damage evaluation process can be roughly described by a structural degradation flow curve in a parameter interval, as shown in Fig 2.

EFs cause damage, thus EFs can be regarded as causal events, and damage can be regarded as resultant events. In Fig 2, R is structural strength degree. t_p and t_q are the start point of the causal and resultant event, respectively. v is the retention parameter. Resultant event occurrence under the conditions of certain causal events can be reflected by the cumulation of degradation flow curve. To evaluate damage associated with external stimuli and sensor characteristics, we simplify the degradation factors presented in [24]. Let the causal events set be $\boldsymbol{C}\{C_1, C_2, \ldots C_{cn}\}$, and the damage events set be $\boldsymbol{D}\{D_1, D_2, \ldots D_{dn}\}$. Then the DF from causal event C_j to D_r damage event can be modelled as:

$$\phi_{jr} = \int_{t_p}^{t_q} \exp(-t/v). \quad (2)$$

When the interval between causal and resultant event is small, the structural damage is slight due to the tiny

external stimulus. The integral value in this case is also small, and vice versa. Thus, DF is directly proportional to the conditional probability of damage. Structural damage has continuous and accumulative effects; the next damage is developed from the previous damage. Hence, a logical relationship exists between the continuous signal wave parameters. The TFW sequence is defined as the difference between the start of the causal and the resultant signals, i.e. $\nabla t_{gh} = b_{gh} - b_{g(h-1)}$, where $g \in [1, m]$, $h \in [1, l-1]$. The parameter interval matrix can be obtained as follows:

$$\nabla t = \begin{bmatrix} \nabla t_{11} & \nabla t_{21} & \dots & \nabla t_{m1} \\ \nabla t_{12} & \dots & \dots & \dots \\ \dots & \dots & \dots & \dots \\ \nabla t_{1(l-1)} & \dots & \dots & \nabla t_{m(l-1)} \end{bmatrix} = \begin{bmatrix} b_{12} - b_{11} & b_{22} - b_{21} & \dots & b_{m2} - b_{m1} \\ b_{13} - b_{12} & \dots & \dots & \dots \\ \dots & \dots & \dots & \dots \\ b_{1l} - b_{1(l-1)} & \dots & \dots & b_{ml} - b_{m(l-1)} \end{bmatrix}. \tag{3}$$

Then, the DF matrix can be calculated based on the parameter interval, as follows:

$$\phi = \begin{bmatrix} \phi_{11} & \phi_{21} & \dots & \phi_{m1} \\ \phi_{12} & \dots & \dots & \dots \\ \dots & \dots & \dots & \dots \\ \phi_{1(l-1)} & \dots & \dots & \phi_{m(l-1)} \end{bmatrix}. \tag{4}$$

Each element of the DF matrix represents the system health degradation factor of a particular causal event to a resultant event.

C. STRUCTURAL DAMAGE INFORMATION ENTROPY (SDIE) VECTOR

Information entropy is a measurement of uncertainty. For a random variable vector X, its information entropy is defined as:

$$H(X) = -\sum P(x_d) \times \log(P(x_d)), d \in N, \tag{5}$$

where x_d is a random variable component, $P(x_d)$ is the probability of x_d. Structural damage is a stochastic problem. The combined strength changes from causal event C_j and damage event D_r can be expressed as

$$\phi_r = \phi_{1,r} + \phi_{2,r} + \dots + \phi_{cn,r}, \tag{6}$$

and

$$\phi_j = \phi_{j,1} + \phi_{j,2} + \dots + \phi_{j,dn}, \tag{7}$$

where cn is the number of causal events, dn is the number of damage resultant events. The likelihood of cause and resultant events can be represented as the probability of the joint events:

$$P\left(\phi_{jr}\right) = P(C_j, D_r), \tag{8}$$

where $P(C_j, D_r)$ is the probability that causal event C_j and resultant event D_r occur simultaneously. From the perspective of uncertainty, the probability of a damage resultant event is (causal events can also be expressed as such, and will not be repeated here):

$$\begin{aligned} P(\phi_r) &= k_1 \times P(\phi_{1r}) + k_2 \times P(\phi_{2r}) + \dots k_{cn} \times P(\phi_{(cn)r}) \\ &= k_1 \times P(C_1, D_r) + k_2 \times P(C_2, D_r) + \dots \\ &\quad + k_{cn} \times P(C_{cn}, D_r), \end{aligned} \tag{9}$$

where $P(\phi_r) \in [0, 1]$. $\boldsymbol{k}$ is the contribution weight vector from each causal event to the damage result and can be different under diverse situations according to the environmental disparities. For example, when the structural material is hydrophilic, the humidity factor should be given a lower and a higher weight in a dry and humid environment, respectively. Expanding the formula based on the probability calculation criteria, we get:

$$\begin{aligned} P(\phi_r) &= k_1 \times P(C_1) \times P(D_r|C_1) + k_2 \times P(C_2) \times P(D_r|C_2) + \dots \\ &\quad + k_{cn} \times P(C_{cn}) \times P(D_r|C_{cn}) \\ &= \sum_{gm=1}^{cn} k_{gm} \times P(C_{gm}) \times P(D_r|C_{gm}), \end{aligned} \tag{10}$$

where $P(D_r|C_{cn})$ is the conditional probability that the resultant event D_r occurs given causal event C_{cn}. Damage occurrence is uncertain. The uncertainty caused by multiple EF has a cumulative effect, which determines whether the damage authentically occurs. Let the causal event leading to a resultant event be a random variable, the uncertainty of damage events set $\boldsymbol{D}$ can be expressed by SDIE as:

$$H(D) = -\sum P(\phi) \times \log(P(\phi)). \tag{11}$$

Expand it further as:

$$\begin{aligned} H(D) &= -\sum_{r=1}^{dn} \sum_{j=1}^{cn} P(\phi_{jr}) \times \log(P(\phi_{jr})) \\ &= -\sum_{j=1}^{cn} P(\phi_j) \times \log(P(\phi_j)) \\ &= -\sum_{j=1}^{cn} k_j \times P(C_j) \times P(D|C_j) \times \log(k_j \times P(C_j) \times P(D|C_j) \\ &= -\sum_{r=1}^{dn} \sum_{j=1}^{cn} k_{jr} \times P(C_j) \times P(D_r|C_j) \\ &\quad \times \log(k_{jr} \times P(C_j) \times P(D_r|C_j), \end{aligned} \tag{12}$$

where k_{jr} is the contribution weight from each causal event to resultant event. $P(D_r|C_j)$ is the damage probability under the condition of causal event. For the probabilistic expression of the DF matrix, normalization scaling factor ***Nor*** is introduced

here, which is expressed as

$$Nor = \begin{bmatrix} 1/\sum_{c=1}^{l-1}\phi_{1c} & 1/\sum_{c=1}^{l-1}\phi_{2c} & \cdots & 1/\sum_{c=1}^{l-1}\phi_{mc} \\ 1/\sum_{c=1}^{l-1}\phi_{1c} & \cdots & \cdots & \cdots \\ \cdots & \cdots & \cdots & \cdots \\ 1/\sum_{c=1}^{l-1}\phi_{1c} & \cdots & \cdots & 1/\sum_{c=1}^{l-1}\phi_{mc} \end{bmatrix}. \quad (13)$$

The original DF matrix is normalized by column, and the result is:

$$\boldsymbol{\phi}^{Nor} = \boldsymbol{\phi} * Nor = \begin{bmatrix} \boldsymbol{\phi}_{11}/\sum_{c=1}^{l-1}\boldsymbol{\phi}_{1c} & \boldsymbol{\phi}_{21}/\sum_{c=1}^{l-1}\boldsymbol{\phi}_{2c} & \cdots & \boldsymbol{\phi}_{m1}/\sum_{c=1}^{l-1}\boldsymbol{\phi}_{mc} \\ \boldsymbol{\phi}_{12}/\sum_{c=1}^{l-1}\boldsymbol{\phi}_{1c} & \cdots & \cdots & \cdots \\ \cdots & \cdots & \cdots & \cdots \\ \boldsymbol{\phi}_{1(l-1)}/\sum_{c=1}^{l-1}\boldsymbol{\phi}_{1c} & \cdots & \cdots & \boldsymbol{\phi}_{m(l-1)}/\sum_{c=1}^{l-1}\boldsymbol{\phi}_{mc} \end{bmatrix}, \quad (14)$$

where * is the Hadamard operator. The DF reflects the occurrence of resultant events under the conditions of certain causal events. Thus, the normalized DF indicates the magnitude of damage probability caused by the causal event. SDIE vector can be expressed as

$$H(D) = -\sum_{j=1}^{cn}\sum_{r=1}^{dn} k_{jr} \times P(C_j) \times \phi_{jr}^{Nor} \times \log(k_{jr} \times P(C_j) \times \phi_{jr}^{Nor}). \quad (15)$$

DFs are summed due to the cumulative effect, and the SDIE is expressed as the damage uncertainty under the various parameters, as

$$H(D) = -\sum_{y=1}^{l-1} k_p \times P(C_p) \times \phi_{py}^{Nor} \times \log(k_p \times P(C_p) \times \phi_{py}^{Nor}), p \in [1, m]. \quad (16)$$

To show the probability uncertainty under each parameter, the SDIE is expressed as

$$H(D) = \{H^{C_1}(\phi), H^{C_2}(\phi), \ldots, H^{C_{cn}}(\phi)\}. \quad (17)$$

The accumulated damage uncertainty can be expressed as

$$Hv = \sum H(D) = \sum_{s=1}^{cn} H^s(\phi). \quad (18)$$

SDIE can assess the damage uncertainty of this monitoring signal segment under multi-parameters. The smaller the value, the greater the damage confidence, and the more likely damage is to occur.

D. SHM CAUSE AND EFFECT ANALYSIS

1) FATIGUE ASSESSMENT

Local energy is a significant parameter of damage assessment in structural mechanics. In [25], an energy-based rock structural damage assessment index was proposed, which consists of three energy indicators: additional energy required (dW_x), unloading elastic energy (dW_{ue}), and dissipation energy of pre-peak stage (dW_d). The expressions are as follows:

$$dW_x = (\sigma_P^2 - \sigma_R^2)/2M, \quad (19)$$

$$dW_{ue} = (\sigma_P^2 - \sigma_R^2)/2E, \quad (20)$$

$$dW_d = \int_0^{\varepsilon_P} \sigma_k d\varepsilon_k - \sigma_P^2/2E, \quad (21)$$

where σ_P is the peak stress, σ_R is the residual stress, σ_k is the pre-peak stress curve function, M is the post-peak modulus, E is the elastic modulus, ε_P is the strain corresponding to the peak stress, ε_k is the strain curve function. Combining these three energy indicators, the damage can be assessed as

$$D_a = dW_x/(dW_{ue} + dW_d) = \frac{E(\sigma_P^2 - \sigma_R^2)}{M}/(2E \times \int_0^{\varepsilon_P} \sigma_k d\varepsilon_k - \sigma_R^2). \quad (22)$$

The integral term approximates to the accumulation of the product of stress and strain, as

$$\int_0^{\varepsilon_P} \sigma_k d\varepsilon_k \propto \sum \sigma_k \times \varepsilon_k, \quad \varepsilon_k \in [0, \varepsilon_p], \ \sigma_k \in [0, \sigma_p]. \quad (23)$$

It is widely accepted that the trend of rock strain and crack propagation obeys a Weibull Distribution [26]. The probability density function (PDF) of strain can be expressed as

$$f(\varepsilon) = \alpha\beta \times (\varepsilon\beta)^{\alpha-1} \times \exp[-(\varepsilon\beta)^{\alpha}], \quad (24)$$

where α is sharp parameter, β is scale parameter. By integrating both sides of (24), the distribution probability of strain can be expressed as follows:

$$F(\varepsilon) = \int_0^{\varepsilon_P} f(\varepsilon) d\varepsilon = 1 - \exp[-(\varepsilon\beta)^{\alpha}], \quad \varepsilon \in [0, \varepsilon_p]. \quad (25)$$

Assume the probability distribution of the stress curve is $F(\sigma)$, the damage probability value can be expressed as

$$Pv(Da) = \frac{E(\sigma_P^2 - \sigma_R^2)}{M} / \left(2E \times F(\varepsilon) \times F(\sigma) - k_R \times \sigma_R^2\right), \quad (26)$$

where k_R is the scale coefficient. SDIE represents damage probability. Many experimental studies have shown that structural damage is positively correlated with stress values under constant conditions [27]–[29]. Thus, SDIE can be employed to replace stress distribution probability. Although the residual stress fluctuates with the external environment, it has a small variation range compared with external stress

and is not dominant, hence, its influence can be ignored [30]. M and E are constants which can be ignored under a given physical state. For describing the damage probability quantitatively, the fatigue index of D_r can be defined as follows:

$$\varphi(D_r) = \frac{\sigma_P^2}{K_g \times Hv \times (1 - \exp(-(\varepsilon\beta)^\alpha))}, \tag{27}$$

where K_g is the adjustment coefficient. The structural fatigue state under multi-parameter synergy can be described through this index.

2) CAUSE TRACING

The SDIE vector reflects the damage uncertainty under various parameter components. Let the parameter be an EF, and each SDIE component be the posterior probability of damage occurrence under this EF. The probability of contribution of EF under this damage result can be calculated using Bayesian method. The damage causal strength index of C_j can be defined as follows:

$$\theta(C_j) = \frac{P(C_j) \times H^s(\phi)}{\sum_{f=1}^{l-1} P(C_f) \times H^f(\phi)}, \tag{28}$$

where $H^s(\phi)$ is the sth element of the SDIE vector, $P(C_j)$ is the priori probability of C_j. The EF most likely to cause damage can be identified from the multi-dimensional sensor information through this index. Thus, incentive matching and source localization can be achieved.

III. EXPERIMENT

A. EXPERIMENT SYSTEM

1) SANDSTONE FATIGUE ASSESSMENT BASED ON AE

Sandstone has good hydrophilicity due to the transparent internal cracks, thus moisture content has a great influence on its structural stability. Many studies indicate that with the increase of moisture content, sandstone structure tends to be unstable and it is likely to collapse [31]–[33]. This structural anomaly can be clearly reflected in AE signal mode. There will be significant change in AE parameters such as energy, ring count and so on along with disparities of moisture content. Moisture content is a crucial driving factor for AE parameter fluctuation. In order to simplify the experiment process, other driving factors are ignored in this experiment. The moisture weighing method was used to simulate the damage and generate a series of causal events. Sandstones with different moisture content were used as experimental samples to justify these changes for SHM. Uniaxial pressure was applied to excite AE events, and the damage state was assessed by AE signal. This experimental system consisted of a hydraulic device, AE sensors, an AE signal process system and a host computer. The system schematic and scene are shown in Fig 3(a) and (b) respectively. The AE sensors are resonant piezoelectric produced by Pengxiang Technology Company in Changsha,

China, and the model number is PXR03. There are buffer and voltage comparison modules in AE acquisition system.

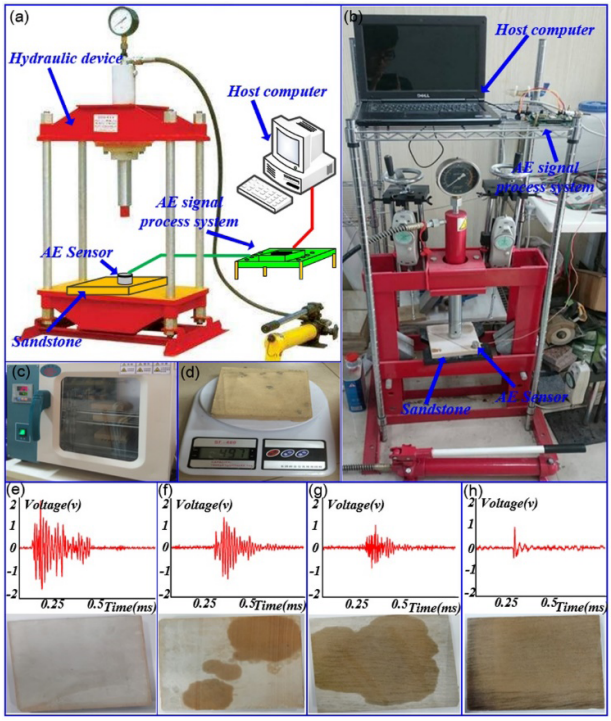

FIGURE 3. (a) System schematic of fatigue assessment experiment. (b) Real scene of fatigue assessment experiment. (c) Drying oven. (d) Electronic scale. (e) Dry samples and typical AE signal. (f) Samples with 25% moisture content and typical AE signal. (g) Samples with 75% moisture content and typical AE signal. (h) Saturated samples and typical AE signal.

Thus, only the maximum AE event would be captured when simultaneous AE overlap. This experiment simulated different damage levels by accurately controlling the moisture content. Four moisture contents, measured by the level of saturation, namely 0% (dry), 25%, 75% and 100% (saturated), were used. The drying oven and electronic scale are shown in Fig 3(c) and (d). The samples with diverse moisture contents and the typical AE signals are shown in Fig 3(e)-(h). It is apparent that the time-domain energy characteristics, such as amplitude, powerful duration etc., of dry samples are more intense than in saturated samples. The AE signal becomes more stable when humidity increases. First, internal energy accumulates under loading. Microcracks emerge when rock particles overcome the bonding energy [34], [35]. Cracks extend further under the rock strain energy effect. The particle friction becomes influential from that point, and its proportion increases along with the growth of cracks. The strain energy and bonding energy releases drastically when loading reaches peak value. At the same time, friction energy enhances rapidly. Particle friction, which is dominant during the crack extension, is weakened by moisture. Thus, the AE signal enters a smooth fluctuation state.

2) TRUSS DAMAGE LOCATING

The basement can be damaged by external force, environmental erosion and so on, which affects the stability of the

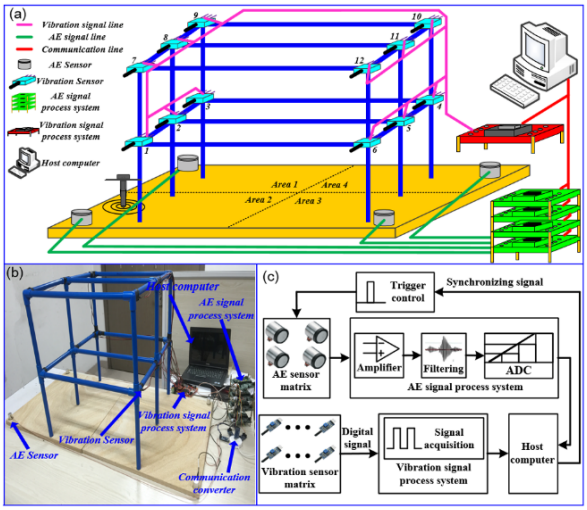

FIGURE 4. (a) The system schematic of damage location experiment. (b) Real scene of damage location experiment. (c) The signal flow.

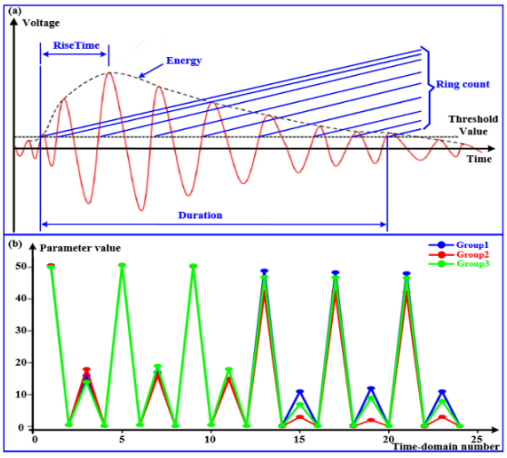

FIGURE 5. (a) Definitions of AE parameters. (b) Time-domain feature waves.

superstructure. Trusses are widely used structures in many infrastructure engineering fields, such as large-span factories, exhibition halls, etc. The rods in a truss structure are mainly subjected to tension and pressure. The shear force distribution and bending moment inside the structure can be balanced using appropriate deployment. Therefore, a truss has great stability and anti-interference. Besides, sandstone is a sedimentary rock with good hydrophilicity and brittleness. Moisture content controlling and AE generation experiments are easy to carry out. Thus, a sandstone-truss structure was suitable as the experimental platform. Damage occurs randomly in structural engineering. The analysis of multiple types information can obtain a more accurate locating. The fusion of acoustic emission and vibration sensor is conducted in this research. The arrival time interval of vibration and acoustic emission signal is the original basis in the damage causal tracing algorithm. Sensors should be installed in reliable positions to avoid noise interference and to obtain stable monitoring data. This experiment simulated a mainstream rock-truss form building. A platform consisting of a sandstone basement and a polyvinyl chloride (PVC) truss was built. The system schematic and experiment scene are shown in Fig 4 (a) and (b) respectively. The basement was divided into four areas, and a collision was applied to the second area to simulate the damage. AE sensors were installed around the basement sandstone to acquire AE signal. The arrive time parameter was extracted as a causal event. Vibration sensors were deployed at each node of the truss. The vibration signal was used as a resultant event. The damage to the basement was located through the causal strength index. The signal flow is shown in Fig 4 (c). The AE signal process mainly included the steps of amplification, filtering, and Analog/Digital (AD) conversion. The magnitude of arrive time parameter was tiny. For accurate timing synchronization, Altera cyclone 3 was used as the core processor to arrange an independent hardware trigger line. The vibration signal processing system set interruption time through the MSP430 internal counter. The number of interruptions were recorded, and the vibration sensing time with unified standard was acquired.

B. DISCUSSION

1) DAMAGE ASSESSMENT

There are various AE parameters, among which energy, duration, ring count and rise time are widely utilized in SHM, hence they are taken as the criteria in this experiment. The definitions of parameters are shown in Fig 5(a). First, uniaxial pressure was applied to all 9 dry samples, and 3 AE signals were collected for each sample. Then, 3 samples were randomly selected to control the moisture content to 25%, 75% and 100%, respectively, and 3 AE signals were collected for each sample again. The AE parameters were calculated to form a TFW. For the 3 samples with varying moisture content as examples, the TFW is shown in Fig. 5(b), where the abscissa is time domain number.

The change characteristics of AE parameters were reflected clearly in Fig. 5 (b). Overall, TFW turns to a trend with decreased fluctuation and reduced amplitude with the increase of moisture content. As shown in the first half of the waveform, the differences of AE parameters are close in dry state. The parameter values have overlap, and the change law is difficult to describe. The valid period characteristics of AE signal is weakened due to the softening effect of moisture. When moisture content rises (the second half of TFW), the gaps emerge increasingly, especially in the small-value parameters. Besides, the higher the moisture content, the more obvious the gaps are.

The retention parameter describes the decreasing rate of structural reliability. To make the subsequent DF calculation more reasonable, suitable v was identified through comparative experiments using the energy parameter. The time intervals of the energy parameter were taken to obtain DF (Fig 6) with different v ranging from 1 to 100.

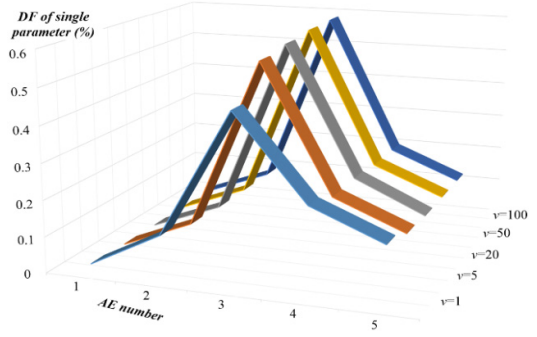

FIGURE 6. DFs of a single parameter under different v.

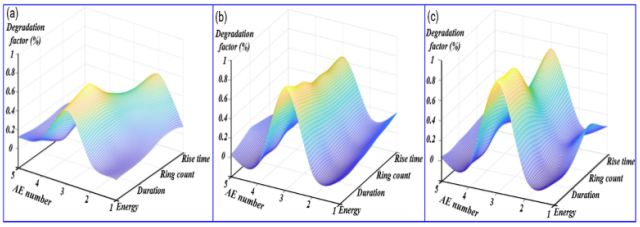

FIGURE 7. (a) Normalized DF matrices of sample with 25% moisture. (b) Normalized DF matrices of sample with 75% moisture. (c) Normalized DF matrices of sample with 100% moisture.

Fig 6 shows that the DF of the energy parameter has a gradually slowing upward trend. DF may be unrecognizable if v is too small. The increasing rate of DF slows down when v is more than 20. Thus, the retention parameter v was set to 20 in this study. 6 AE signals were collected for each sample. That is, 5 sets of parameter intervals were obtained. The number of AE parameters was 4, thus the dimension of DF matrix was 4*5. The normalized DF matrices of the 3 experimental samples are shown in Fig 7, where (a)-(c) respectively correspond to the moisture content of 25%, 75% and 100%.

Fig 7 shows that the mutations of strength state were indicated clearly in DF matrix elements. The third AE event (i.e. the third column of the matrix) was the sampling time when moisture changed. For all samples, the DF peaks occur when the state turns from dry to damp. Moisture weakens the friction between rock particles. Subsequently, AE signal tends to be less strong. The values of parameters such as energy, duration, and rise time accordingly decline. The DF fluctuation of the sample with 25% moisture content was more stable than that of the saturated sample. Besides, moisture has no significant impact on the frequency characteristics, thus, the mutation is not obvious for the ring count parameter.

The causal event in this experiment is parameter value change, and the resultant event is moisture damage. Let the contribution weight k be 1 since the above four AE parameters have no significant difference in sandstone moisture damage assessment. As the damage reflected in each parameter is same, the prior probability $P(C)$ is defined as 1. The SDIE

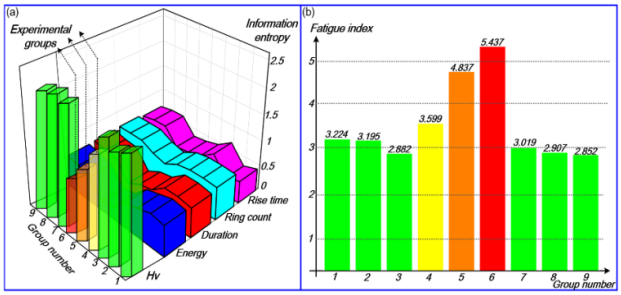

FIGURE 8. (a) The structural damage information entropies of the experimental groups and the dry control groups. (b) The fatigue index results.

of the experimental groups and the dry control groups are shown in Fig 8 (a). SDIE indicates the uncertainty of moisture damage through the causal reasoning analysis. The probability of damage would be higher if internal rock particles are softened by moisture, and the damage uncertainty would be lower. It is obvious that the SDIE of the 3 moisture damage groups are significantly lower than the control groups. The saturated sample was the most likely to have damage (i.e. had the lowest damage uncertainty), and the SDIE was smallest. SDIE value and moisture content are inversely related.

It is known from the Kaiser effect that the stress which excites AE has a memory characteristic [36]. Although the subsequent uniaxial stress changes, the stress value fluctuates weakly due to the irreversibility of AE [37]. Thus, the first stress that causes damage and excites AE can be considered as the peak stress. Sandstone has the characteristics of brittleness and small elastic deformation. Peak stress was set to 52MPa according to the experimental study [38] on the relationship between stress and AE. The values of α and β are usually determined by fitting in practical applications. Here, α and β were set to 0.8 and 3.125, respectively based on the sandstone research in literature [39]. The cause of damage in this experiment was only the moisture-bearing effect, and the comparison benchmark was equal. K_g was taken to be 1 to simplify the calculation. In [40], the strain rate inflection point of sandstone was obtained under creep uniaxial compression conditions, which was the moment of damage occurrence. The Kaiser effect explains the overlap between the damage occurrence and AE events, thus the strain value was set to $5.2*10^{-3}$. The fatigue degree results are shown in Fig 8 (b).

Fig 8 (b) shows that the fatigue degree of the dry groups (green cylinder) is around 3. The fatigue degrees of the damaged samples are apparently larger than dry groups. As the moisture content increases, the fatigue index shows an upward trend. These disparities are consistent with the experimental settings. The moisture softening effect on sandstone is demonstrated and the rationality of this method is supported.

C. DAMAGE LOCATING

The vibration signal is digital, and the TFW value is the same with the origin signal, thus it is not described here. The time

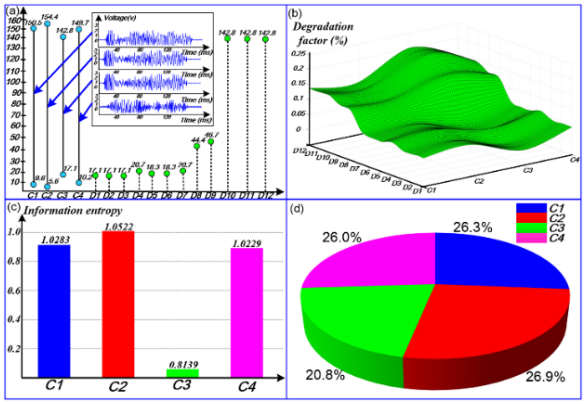

FIGURE 9. (a) The parameter interval of causal and resultant event. (b) Normalized DF matrix. (c) Results of SDIE. (d) The causal strength index result.

interval of AE is taken as the parameter interval. Since the AE signal and vibration signal are of different magnitudes, the resultant event needs to be normalized. Let C'_{sta} and C'_{end} be the maximum start time and the minimum end time of the causal event, respectively. D_{min} and D_{max} are the minimum and maximum values of the resultant event respectively. The normalized formula for D_r is

$$D_r^{Nor} = C'_{sta} + (D_r - D_{\min}) \times \frac{C'_{end} - C'_{sta}}{D_{\max} - D_{\min}}. \quad (29)$$

The original AE signal, normalized AE parameter interval, and the vibration signal time interval are shown in Fig 9(a). The terminal signal collected by sensors is composed of effective AE signal and unpredictable noise. Besides, sandstone has anisotropy, and the wave refraction has a negative impact on the signal shape during the propagation process. Thus, the AE signals captured by the four sensors are discrepant even if the damage source is the same. The normalized DF matrix is shown in Fig 9(b). Fig 9(b) indicates that the DF values vary greatly with the different installation positions of the AE and vibration sensors. Overall, the crests appear in positions far away from damage, and the troughs appear in positions close to damage. This is because the arrival time of the signal is longer when the distance between sensor and damage position is further. Accordingly, the contribution of location probabilities is smaller in causal reasoning. Prior probability $P(C)$ for each causal event was set as 1. The SDIE and causal strength index are shown in Fig 9 (c) and (d), respectively. The maximum values of SDIE and causal strength index both appear in area 2. This result indicates that the causal logics between AE and vibration sensors reached a maximum in area 2. Damage occurs in this area with the largest probability based on the fusion of multiple sensor information. The location output is consistent with the experimental settings, and the feasibility is verified.

IV. CONCLUSION

This paper has proposed a structural damage cause-and-effect analysis method based on parameter information entropy for structural health monitoring. A TFW is defined to collect the parameter information during the entire time sequence. The difference between adjacent parameters is used to obtain the parameter interval. Then the DF matrix has been developed to reflect the structural strength degradation due to the harsh monitoring conditions. The logical association between causal and resultant events is decomposed and combined from a probabilistic perspective. The normalized degradation factor is taken as the conditional probability. The concept of information entropy has been adopted to form an SDIE vector to analyse the uncertainty between damage event and EF. According to the local energy and stress-strain probability distribution theory, a novel fatigue index has been introduced to facilitate the damage assessment. A causal strength index has been presented to locate the most likely damage cause based on Bayesian method. This method intelligently exploits monitoring data. The advantages are as follows:

a). The assessment method is totally data-driven. Damage occurrences are analyzed based on probability uncertainty without the need of complex multidisciplinary knowledge. Thus, it is effective with equipment scalability and portability.

b). Multidimensional AE parameters are applied synergistically, and the subjectivity of expert experience can be avoided during the parameter selection.

c). Undesirable issues concerning monitoring environment, such as sensor aging, reliability reduction and so on, are considered in the evaluation of sensor output characteristics.

In the damage assessment experiment, the TFW of samples with different moisture damage shows a significant disparity. The DF changes intensely when the moisture content increases. SDIE quantitatively describes the difference of damage degree. In the damage cause location experiment, despite the difference in arrive time of each sensor being tiny due to the narrow basement, the causal strength index locates the most likely damage cause.

This study has some limitations: (1) There are lots of driving factors that can lead to AE signal change, and moisture content is one of them. The parameters suitable for causal reasoning may change under multi-driving factor effects. (2) The prior probability used in the experiment is 1 as no literature offers detailed weight differences of AE parameters. Our future work may concentrate on addressing the limitations mentioned above. Diverse damage driving factor experiments would be conducted to generate more causal events and determine the suitable AE parameter types. A massive monitoring database would be built through more AE excitation experiments. The prior probability information would be explored using intelligent algorithms.

REFERENCES

[1] L. E. Mujica, J. Vehí, W. Staszewski, and K. Worden, "Impact damage detection in aircraft composites using knowledge-based reasoning," *Struct. Health Monit.*, vol. 7, no. 3, pp. 215–230, Sep. 2008.

[2] Y. Bao, Y. Yu, H. Li, X. Mao, W. Jiao, Z. Zou, and J. Ou, "Compressive sensing-based lost data recovery of fast-moving wireless sensing for structural health monitoring," *Struct. Control Health Monit.*, vol. 22, no. 3, pp. 433–448, Mar. 2015.

[3] M. Z. A. Bhuiyan, J. Wu, G. Wang, and J. Cao, "Sensing and decision making in cyber-physical systems: The case of structural event monitoring," *IEEE Trans. Ind. Informat.*, vol. 12, no. 6, pp. 2103–2114, Dec. 2016.
[4] D. Lockner, "The role of acoustic emission in the study of rock fracture," *Int. J. Rock Mech. Mining Sci. Geomech. Abstr.*, vol. 30, no. 7, pp. 883–899, Dec. 1993.
[5] K. Tao and W. Zheng, "Real-time damage assessment of hydrous sandstone based on synergism of AE-CT techniques," *Eng. Failure Anal.*, vol. 91, pp. 465–480, Sep. 2018.
[6] R. Janeliukstis and S. Kaewunruen, "A novel separation technique of flexural loading-induced acoustic emission sources in railway prestressed concrete sleepers," *IEEE Access*, vol. 7, pp. 51426–51440, 2019.
[7] S. R. Saufi, Z. A. B. Ahmad, M. S. Leong, and M. H. Lim, "Low-speed bearing fault diagnosis based on ArSSAE model using acoustic emission and vibration signals," *IEEE Access*, vol. 7, pp. 46885–46897, 2019.
[8] K. He and X. Li, "Time–frequency feature extraction of acoustic emission signals in aluminum alloy mig welding process based on SST and PCA," *IEEE Access*, vol. 7, pp. 113988–113998, 2019.
[9] X.-P. Zhang, Q. Zhang, and S. Wu, "Acoustic emission characteristics of the rock-like material containing a single flaw under different compressive loading rates," *Comput. Geotech.*, vol. 83, pp. 83–97, Mar. 2017.
[10] S. A. Shevchik, F. Saeidi, B. Meylan, and K. Wasmer, "Prediction of failure in lubricated surfaces using acoustic time–frequency features and random forest algorithm," *IEEE Trans. Ind. Informat.*, vol. 13, no. 4, pp. 1541–1553, Aug. 2017.
[11] R. P. Dalton, N. Cawley, and M. J. Lowe, "Propagation of acoustic emission signals in metallic fuselage structure," *IEE Proc.-Sci., Meas. Technol.*, vol. 148, no. 4, pp. 169–177, Jul. 2001.
[12] A. Carpinteri, G. Lacidogna, and N. Pugno, "Structural damage diagnosis and life-time assessment by acoustic emission monitoring," *Eng. Fract. Mech.*, vol. 74, nos. 1–2, pp. 273–289, Jan. 2007.
[13] M. M. R. Taha, A. Noureldin, J. L. Lucero, and T. Baca, "Wavelet transform for structural health monitoring: A compendium of uses and features," *Struct. Health Monit.*, vol. 5, no. 3, pp. 267–295, 2006.
[14] A. El-Shafie, A. Noureldin, D. McGaughey, and A. Hussain, "Fast orthogonal search (FOS) versus fast Fourier transform (FFT) as spectral model estimations techniques applied for structural health monitoring (SHM)," *Struct. Multidisciplinary Optim.*, vol. 45, no. 4, pp. 503–513, 2012.
[15] H. Sohn, D. W. Allen, K. Worden, and C. R. Farrar, "Statistical damage classification using sequential probability ratio tests," *Struct. Health Monit.*, vol. 2, no. 1, pp. 57–74, 2003.
[16] H. Cui, X. Xu, W. Peng, Z. Zhou, and M. Hong, "A damage detection method based on strain modes for structures under ambient excitation," *Measurement*, vol. 125, pp. 438–446, Sep. 2018.
[17] M. F. Shamsudin, C. Mares, C. Johnston, Y. Lage, G. Edwards, and T.-H. Gan, "Application of Bayesian estimation to structural health monitoring of fatigue cracks in welded steel pipe," *Mech. Syst. Signal Process.*, vol. 121, pp. 112–123, Apr. 2019.
[18] A. K. Das, T. T. Lai, C. W. Chan, and C. K. Leung, "A new non-linear framework for localization of acoustic sources," *Struct. Health Monit.*, vol. 18, no. 2, pp. 590–601, 2018.
[19] F. Zhu, Z. Deng, and J. Zhang, "An integrated approach for structural damage identification using wavelet neuro-fuzzy model," *Expert Syst. Appl.*, vol. 40, no. 18, pp. 7415–7427, 2013.
[20] H. Salehi, S. Das, S. Chakrabartty, S. Biswas, and R. Burgueño, "Damage identification in aircraft structures with self-powered sensing technology: A machine learning approach," *Struct. Control Health Monit.*, vol. 25, no. 12, p. e2262, 2018.
[21] C. Zhang, L. Cheng, J. Qiu, H. Ji, and J. Ji, "Structural damage detections based on a general vibration model identification approach," *Mech. Syst. Signal Process.*, vol. 123, pp. 316–332, May 2019.
[22] F. Magalhães, A. Cunha, and E. Caetano, "Vibration based structural health monitoring of an arch bridge: From automated OMA to damage detection," *Mech. Syst. Signal Process.*, vol. 28, pp. 212–228, Apr. 2012.
[23] A. Deraemaeker, E. Reynders, G. De Roeck, and J. Kullaa, "Vibration-based structural health monitoring using output-only measurements under changing environment," *Mech. Syst. Signal Process.*, vol. 22, no. 1, pp. 34–56, 2008.
[24] K. Tao and W. Zheng, "Structural damage location and evaluation model inspired by memory and causal reasoning of the human brain," *Struct. Control Health Monit.*, vol. 25, no. 11, p. e2249, 2018.
[25] C. Ai, J. Zhang, Y.-W. Li, J. Zeng, X.-L. Yang, and J.-G. Wang, "Estimation criteria for rock brittleness based on energy analysis during the rupturing process," *Rock Mech. Rock Eng.*, vol. 49, no. 12, pp. 4681–4698, Dec. 2016.
[26] Z. L. Wang, H. Shi, and J. G. Wang, "Mechanical behavior and damage constitutive model of granite under coupling of temperature and dynamic loading," *Rock Mech. Rock Eng.*, vol. 51, no. 10, pp. 3045–3059, 2018.
[27] D. Ai, Y. Zhao, Q. Wang, and C. Li, "Experimental and numerical investigation of crack propagation and dynamic properties of rock in SHPB indirect tension test," *Int. J. Impact Eng.*, vol. 126, pp. 135–146, Apr. 2019.
[28] M. Cai, P. K. Kaiser, Y. Tasaka, T. Maejima, H. Morioka, and M. Minami, "Generalized crack initiation and crack damage stress thresholds of brittle rock masses near underground excavations," *Int. J. Rock Mech. Mining Sci.*, vol. 41, no. 5, pp. 833–847, 2004.
[29] Y. Li, D. Jia, Z. Rui, J. Peng, C. Fu, and J. Zhang, "Evaluation method of rock brittleness based on statistical constitutive relations for rock damage," *J. Petroleum Sci. Eng.*, vol. 153, pp. 123–132, May 2017.
[30] S. Yu, W. Zhu, L. Niu, S. Zhou, and P. Kang, "Experimental and numerical analysis of fully grouted long rockbolt load-transfer behavior," *Tunnelling Underground Space Technol.*, vol. 85, pp. 56–66, Mar. 2019.
[31] D. S. Yang, M. Bornert, S. Chanchole, H. Gharbi, P. Valli, and B. Gatmiri, "Dependence of elastic properties of argillaceous rocks on moisture content investigated with optical full-field strain measurement techniques," *Int. J. Rock Mech. Mining Sci.*, vol. 53, pp. 45–55, Jul. 2012.
[32] L. Girard, S. Gruber, S. Weber, and J. Beutel, "Environmental controls of frost cracking revealed through *in situ* acoustic emission measurements in steep bedrock," *Geophys. Res. Lett.*, vol. 40, no. 9, pp. 1748–1753, 2013.
[33] Y. Nara, K. Morimoto, N. Hiroyoshi, T. Yoneda, K. Kaneko, and P. M. Benson, "Influence of relative humidity on fracture toughness of rock: Implications for subcritical crack growth," *Int. J. Solids Struct.*, vol. 49, no. 18, pp. 2471–2481, 2012.
[34] N. Cho, C. D. Martin, and D. C. Sego, "A clumped particle model for rock," *Int. J. Rock Mech. Mining Sci.*, vol. 44, no. 7, pp. 997–1010, 2007.
[35] J. F. Hazzard, R. P. Young, and S. C. Maxwell, "Micromechanical modeling of cracking and failure in brittle rocks," *J. Geophys. Res.-Solid Earth*, vol. 105, no. B7, pp. 16683–16697, 2000.
[36] Y. L. Chen, M. Irfan, and C. P. Song, "Verification of the kaiser effect in rocks under tensile stress: Experiment using the Brazilian test," *Int. J. Geomech.*, vol. 18, no. 7, p. 7, Jul. 2018.
[37] F. X. Passelègue, L. Pimienta, D. Faulkner, A. Schubnel, J. Fortin, and Y. Guéguen, "Development and recovery of stress-induced elastic anisotropy during cyclic loading experiment on westerly granite," *Geophys. Res. Lett.*, vol. 45, no. 16, pp. 8156–8166, Aug. 2018.
[38] J. Browning, P. G. Meredith, C. E. Stuart, D. Healy, S. Harland, and T. M. Mitchell, "Acoustic characterization of crack damage evolution in sandstone deformed under conventional and true triaxial loading," *J. Geophys. Res.-Solid Earth*, vol. 122, no. 6, pp. 4395–4412, 2017.
[39] A. J. DesRoches, K. E. Butler, and S. Pelkey, "Influence of fracture anisotropy and lithological heterogeneity on wellfield response in a fluvial sandstone aquifer of the Carboniferous Moncton Subbasin, Canada," *Hydrogeol. J.*, vol. 21, no. 3, pp. 559–572, 2013.
[40] Y. Li and C. Xia, "Time-dependent tests on intact rocks in uniaxial compression," *Int. J. Rock Mech. Mining Sci.*, vol. 37, no. 3, pp. 467–475, 2000.

KAI TAO received the B.S. degree in electrical engineering and management from the Qingdao University of Technology, Qingdao, China, in 2015. He is currently pursuing the Ph.D. degree in instrument science and technology with Chongqing University.

He was an University Associate Researcher with the University of Tasmania, Australia, from 2018 to 2019. His research interests mainly focus on structural health monitoring and advance signal processing.

WEI ZHENG (M'10) received the B.S. degree in automatic control engineering from Beihang University, Beijing, China, in 1998, and the M.S. degree in navigation, guidance, and control from the China Academy of Launch Vehicle Technology, Beijing, in 2004, and the Ph.D. degree in instrument science and technology from Beihang University, Beijing, in 2008.

From 2008 to 2010, he was a Postdoctoral Research Fellow with Chongqing University, China, where he is currently a Professor. His researches focus on structural health monitoring, advance signal processing, intelligent instrument, and automatic testing systems.

DANCHI JIANG (M'96) received the bachelor's degree in mathematics from Wuhan University, China, the master's degree in control systems and applications from East China Normal University, China, and the Ph.D. degree in systems engineering from The Australian National University.

His current research interests include systems engineering and advanced signal processing. He was a recipient of the ADCOS Scholarship from the Australian Agency for International Development, from 1994 to 1998 and the Postdoctoral Research Fellowship from The Chinese University of Hong Kong, from 1996 to 1998. He has been the Stream Chair of Computer Systems Engineering with the School of Engineering and ICT, since 2005.